Chemical Science

EDGE ARTICLE

View Article Online
View Journal | View Issue

Cite this: *Chem. Sci.*, 2016, 7, 3264

Evaluation of the coordination preferences and catalytic pathways of heteroaxial cobalt oximes towards hydrogen generation†

Debashis Basu,‡[a] Shivnath Mazumder,‡[a] Jens Niklas,[b] Habib Baydoun,[a] Dakshika Wanniarachchi,[a] Xuetao Shi,[a] Richard J. Staples,[c] Oleg Poluektov,[b] H. Bernhard Schlegel*[a] and Cláudio N. Verani*[a]

Three new heteroaxial cobalt oxime catalysts, namely $[\mathrm{Co^{III}(prdioxH)(^{4tBu}py)(Cl)}]\mathrm{PF_6}$ (**1**), $[\mathrm{Co^{III}(prdioxH)(^{4Pyr}py)(Cl)}]\mathrm{PF_6}$ (**2**), and $[\mathrm{Co^{III}(prdioxH)(^{4Bz}py)(Cl)}]\mathrm{PF_6}$ (**3**) have been studied. These species contain chloro and substituted *tert*-butyl/pyrrolidine/benzoyl-pyridino ligands axially coordinated to a trivalent cobalt ion bound to the $\mathrm{N_4}$-oxime macrocycle (2*E*,2′*E*,3*E*,3′*E*)-3,3′-(propane-1,3-diylbis(azanylylidene))bis(butan-2-one)dioxime, abbreviated $\mathrm{(prdioxH)^-}$ in its monoprotonated form. Emphasis was given to the spectroscopic investigation of the coordination preferences and spin configurations among the different $3d^6$ $\mathrm{Co^{III}}$, $3d^7$ $\mathrm{Co^{II}}$, and $3d^8$ $\mathrm{Co^{I}}$ oxidation states of the metal, and to the catalytic proton reduction with an evaluation of the pathways for the generation of $\mathrm{H_2}$ *via* $\mathrm{Co^{III}{-}H^-}$ or $\mathrm{Co^{II}{-}H^-}$ intermediates by mono and bimetallic routes. The strong field imposed by the $\mathrm{(prdioxH)^-}$ ligand precludes the existence of high-spin configurations, and 6-coordinate geometry is favored by the $\mathrm{^{LS}Co^{III}}$ species. Species **1** and **3** show a split $\mathrm{Co^{III}/Co^{II}}$ electrochemical wave associated with partial chemical conversion to a $[\mathrm{Co^{III}(prdioxH)Cl_2}]$ species, whereas **2** shows a single event. The reduction of these $\mathrm{Co^{III}}$ complexes yields $\mathrm{^{LS}Co^{II}}$ and $\mathrm{^{LS}Co^{I}}$ species in which the pyridine acts as the dominant axial ligand. In the presence of protons, the catalytically active $\mathrm{Co^{I}}$ species generates a $\mathrm{Co^{III}{-}H^-}$ hydride species that reacts heterolytically with another proton to generate dihydrogen. The intermediacy of a trifluoroacetate-bound $\mathrm{Co^{III}/Co^{II}}$ couple in the catalytic mechanism is proposed. These results allow for a generalization of the behavior of heteroaxial cobalt macrocycles and serve as guidelines for the development of new catalysts based on macrocyclic frameworks.

Received 5th November 2015
Accepted 30th January 2016

DOI: 10.1039/c5sc04214c

www.rsc.org/chemicalscience

Introduction

Research in molecular catalysts for proton and water reduction has been intensive and in recent years special attention was paid to the use of Earth-abundant metals.[1–4] Cobalt ions, with their ability to span redox states from 3+ ($3d^6$) to 1+ ($3d^8$) have been emphasized, and effective catalysts have been designed for both proton and water reduction with oximes.[3] Starting with the adventitious observation by Espenson & Connolly[5] that biomimetic cobalt oximes are capable of proton reduction in acidic organic media, these catalysts figure among the first observed systems and have been extensively scrutinized. In spite of this interest and of available information for individual cobalt oximes,[6] comprehensive spectroscopic studies that interrogate the transformation of oxidation states along the reductive process that leads to the catalytically active $\mathrm{Co^{I}}$ species are rare. Furthermore, the vast majority of studied catalytic systems contain equivalent axial ligands, hereafter called homoaxial, and added complexity is observed when non-equivalent axial ligands are present. These heteroaxial cobalt oximes display two $\mathrm{Co^{III}/Co^{II}}$ redox processes associated with the formation of a new $\mathrm{Co^{III}}$ species in solution. These distinct species yield a monovalent catalyst. A previous study to rationalize this behavior was performed by Gerli and Marzilli[7] where an exclusively electrochemical pathway was proposed, leading to a square planar $\mathrm{Co^{II}}$ species that yields a catalytic 4-coordinate $\mathrm{Co^{I}}$ intermediate. However, both experimental[8,9] and theoretical[6g] evidence suggest that this intermediate requires 5-coordination with *N*-containing donors.

Thus, we propose that a unifying investigation based on UV-visible, nuclear magnetic and electron paramagnetic (NMR & EPR) resonance spectroscopies allied with DFT calculations will

---

[a] *Department of Chemistry, Wayne State University, Detroit, MI 48202, USA. E-mail: cnverani@chem.wayne.edu*

[b] *Chemical Sciences and Engineering Division, Argonne National Laboratory, Argonne, IL 60439, USA*

[c] *Department of Chemistry, Michigan State University, Lansing, MI 48824, USA*

† Electronic supplementary information (ESI) available. CCDC 1434959, 1434960, 1448834 and 1449138. For ESI and crystallographic data in CIF or other electronic format see DOI: 10.1039/c5sc04214c

‡ D. B. and S. M. contributed equally to this work.

allow for the understanding of the coordination preferences of heteroaxial cobalt oxime systems and, therefore, of the behavior of the trivalent, divalent, and monovalent species crucial for catalytic H_2 generation. This knowledge will enable us to chart the transformations that occur during the catalytic cycle addressing the nature of formed hydrides, the viability of proton-coupled electron transfer, the homo or heterolytic nature of hydrogen formation, and the regeneration of the catalyst.

Continuing a long-standing collaboration on cobalt systems,[10] we have recently examined the catalytic activity of cobalt species associated with pendant phenolates[10e] and pyridines.[10f] We have also studied in detail a new pentadentate cobalt oxime system[10g] designed to stabilize the above-mentioned preferential 5-coordination favored by Co^I in catalysts used for proton/water reduction. We observed that upon metal coordination this new oxime incorporates a molecule of water and enables H^+ reduction in presence of weak acids in acetonitrile (CH_3CN).

In this paper we present three new heteroaxial catalysts, namely $[Co^{III}(prdioxH)(^{4tBu}py)(Cl)]PF_6$ (**1**), $[Co^{III}(prdioxH)(^{4Pyr}py)(Cl)]PF_6$ (**2**), and $[Co^{III}(prdioxH)(^{4Bz}py)(Cl)]PF_6$ (**3**), Fig. 1, in which the axial pyridine displays both electron-donating and electron-withdrawing functionalities. We interrogate by concerted experimental and theoretical methods the transformations in nature and coordination preferences associated with the 3+, 2+, and 1+ oxidation states of the metal, and propose a viable catalytic pathway for hydrogen formation. These results are relevant to the development of strategies for the improvement of new catalysts for proton and water reduction based on heteroaxial cobalt macrocycles.

Results and discussion

Synthesis and characterization of 1, 2, and 3

The tetradentate ligand prdioxH$_2$ was obtained by literature methods.[11,12] Complexes **1**, **2**, and **3** were generated by stepwise reaction of $CoCl_2 \cdot 6H_2O$ with the ligand prdioxH$_2$ to obtain the dichloro complex which was further treated with 4-substituted pyridines and KPF_6 to yield **1–3** (Fig. S1†). The FTIR spectra of the complexes reveal a C═N stretching vibration mode associated with the oxime ligand at *ca.* 1600 cm^{-1} and a strong and broad peak around 850 cm^{-1} indicative of the presence of PF_6^- counterions. High-resolution ESI mass spectra (Fig. S2†) display the species $[M]^+$ at 468.1573, 481.1563 and 516.1207 respectively for **1**, **2**, and **3**. Experimental and simulated isotopic distributions are in agreement with the proposed molecular composition. ^{1}H-NMR spectra were taken in CD_3CN and the spectrum for **1** is shown in Fig. 2, and the narrow lines confirm the diamagnetic nature of these species, as associated with a 3d^6 $^{LS}Co^{III}$ ion.

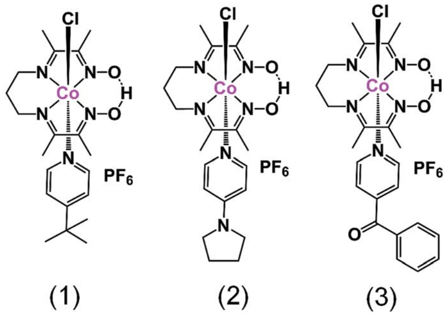

Fig. 1 The mononuclear complexes $[Co^{III}(prdioxH)(^{4tBu}py)(Cl)]PF_6$ (**1**), $[Co^{III}(prdioxH)(^{4Pyr}py)(Cl)]PF_6$ (**2**), and $[Co^{III}(prdioxH)(^{4Bz}py)(Cl)]PF_6$ (**3**).

The spectra show appropriate line-splitting patterns for **1** with four aromatic protons between 6 and 8 ppm originating from the pyridine moiety, one OH proton at 18.85 ppm, six methylene protons between 2.0 and 4.5 ppm and 12 methyl protons between 2.4 and 2.6 ppm. The intense peaks found around 1.3 ppm are from the protons (9H) of the *t*-butyl substituent. Complexes **1** and **3** yielded diffraction-quality crystals whose ORTEP plots are shown in Fig. 3. In both cases a pseudo-octahedral geometry of the cobalt center was found with the oxime ligand occupying the equatorial plane, while chloride and ^{4tBu}pyridine/^{4Bz}pyridine ligands occupy the axial positions. One of the oxime-oxygen atoms remains protonated forming an O–H⋯O hydrogen-bonded macrocyclic framework. The Co–N^{oxime} bond lengths (1.88–1.93 Å) are in excellent agreement with other oxime complexes in the literature.[3c,7] Comparison of the Co–Cl bond length between **1** and **3** reveals a slightly longer bond in **1** (2.2376 Å) than in **3** (2.2336 Å). On the other hand, the bond length between Co and the N^{Py} atom (Co1–N5) is shorter in **1** (1.975 Å) than in **3** (1.990 Å). These results suggest that incorporation of the electron-withdrawing benzoyl substituent on the pyridine ring of **3** weakens the Co–N5 (pyridine) bond and strengthens the Co–Cl bond.

Coordination preferences of different oxidation states in the proton reduction pathway

The 1e$^-$ and 2e$^-$ reduced analogs of **1–3** generated in the electrochemical pathway towards catalysis determine the viability of proton reduction. Therefore, a detailed evaluation of their coordination preferences, spin states, and electronic structures is of the utmost importance in the understanding of catalytic pathways. We probed each of these species by cyclic

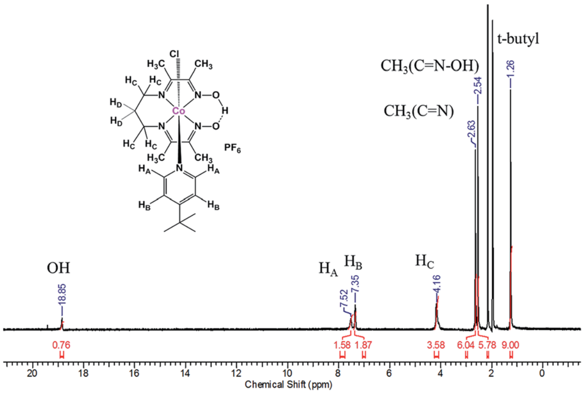

Fig. 2 ^{1}H-NMR spectra of **1** in CD_3CN.

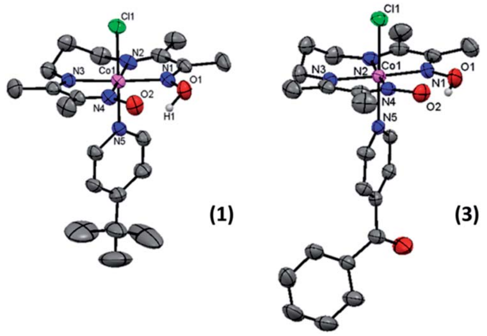

Fig. 3 ORTEP representation of the crystal structures for $[Co^{III}(prdioxH)(^{X}py)(Cl)]^+$ cations in **1** (CCDC 1434960) and **3** (CCDC 1434959) at 50% ellipsoid probability. For **1**: Co(1)–N(1) = 1.903(3); Co(1)–N(2) = 1.917(2); Co(1)–N(3) = 1.914(2); Co(1)–N(4): 1.898(2) = Co(1)–N(5) = 1.975(3); Co(1)–Cl(1) = 2.237(8) Å. For **3**: Co(1)–N(1) = 1.891(3); Co(1)–N(2) = 1.934(3); Co(1)–N(3) = 1.923(3); Co(1)–N(4) = 1.893(3); Co(1)–N(5) = 1.990(3); Co(1)–Cl(1) = 2.2336(11) Å.

voltammetry (CV), ^{1}H-NMR, UV-visible, EPR, and DFT methods aiming to characterize comprehensively the nature of these species.

Redox properties. Complexes **1–3** were investigated by CV in CH_3CN with the resulting traces shown in Fig. 4 and relevant potentials summarized in Table 1. Species **1** revealed two events associated with the Co^{III}/Co^{II} couple at −0.49 V ($E_{p,c}$) and −0.70 V ($E_{1/2}$), similar to the values for a structurally related species,[7] whereas the Co^{II}/Co^{I} process appears at −1.09 V ($E_{1/2}$); all potentials are given *versus* the ferrocene/ferrocenium (Fc/Fc^+) couple. One additional reduction process was found at −2.11 V_{Fc/Fc^+} and may be attributed to the imine/oxime ligand. A similar profile was observed for **3**, while a slightly different behavior was observed for **2** with seemingly only one Co^{III}/Co^{II} event.

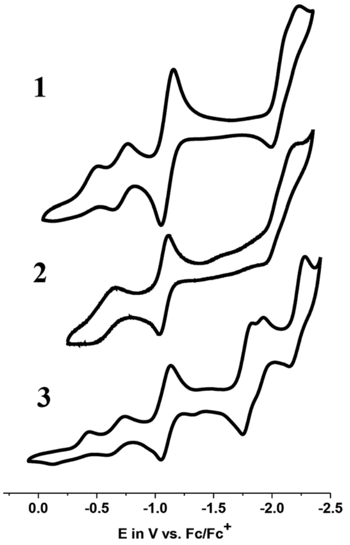

Fig. 4 Cyclic voltammograms of **1**, **2**, and **3** in CH_3CN (supporting electrolyte: $TBAPF_6$; scan rate: 100 mV s^{-1}; glassy C: working electrode; Pt-wire: auxiliary electrode; Ag/AgCl: reference electrode).

In order to check for potential coordination of the solvent CH_3CN, thus generating a new species $[Co^{III}(prdioxH)(CH_3CN)_2]^{2+}$ associated with the second Co^{III}/Co^{II} redox event observed in **1** and **3**, the CV of **1** was repeated in non-coordinating CH_2Cl_2 (Fig. S3†). Both Co^{III}/Co^{II} events persisted, thus ruling out the formation of bis-acetonitrile species. The origin of this second Co^{III}/Co^{II} process will be discussed later.

Electronic properties. Complexes **1–3** are nearly transparent in the visible region (Fig. S4†). A detailed study was conducted with the parent Co^{III} species and Co^{II} and Co^{I} reduced counterparts of **1**, isolated in CH_3CN by bulk electrolysis at −0.46 and −0.95 $V_{Ag/AgCl}$, respectively (Fig. 5). The spectrum of **1** displays a light yellow color and is marked by the absence of charge-transfer (CT) bands characteristic of a $3d^6$ $^{LS}Co^{III}$ center bound to a strong-field π-acceptor ligand framework.[12] The orange Co^{II} species shows a distinct peak at 480 nm ($\varepsilon = 2288$ M^{-1} cm^{-1}) attributed to a metal-to-ligand charge transfer (MLCT) transition. The optical spectrum of the Co^{I} species is tentatively associated with both intraligand charge transfer (ILCT) and MLCT bands at 572 and 685 nm ($\varepsilon = 1738$ and 1570 M^{-1} cm^{-1}), respectively, accounting for the intense dark blue color of the complex. As suggested by Espenson *et al.*[8] the higher orbital energy in the Co^{I} state compared with Co^{II}, shifts the lower energy transition to the region between 500 and 700 nm.

Similar observations were made by Peters *et al.*[9] when studying hydrogen oxidation reactions with Co^{II} homoaxial oxime complexes. The parent yellow solution of Co^{II} species ($\lambda_{max} = 440$ nm) turns to Co^{I} upon hydrogen oxidation. The Co^{I} product exhibited a dark blue color and showed two strong absorption bands between 500 and 700 nm.[9] Eisenberg *et al.*[3h] also detected similar Co^{I} spectra ($\lambda_{max} = 550$, 650 nm) for Co^{II} oxime complexes with homoaxial water ligands and with Pt-chromophore and TEOA as the sacrificial donor in the presence of visible light. Thus, the parent compounds **1–3** seem to allow for reduction to Co^{I} at affordable potentials. Knowledge on the nature of this species is relevant for the understanding of competing mechanisms that precede catalytic proton reduction in acidic organic media.

The coordination environment of the Co^{III} species. Crystal structures combined with ^{1}H-NMR spectroscopy provided the strongest evidence to elucidate the coordination environment for Co^{III} in the parent state. The crystal structure of **1** (Fig. 3) confirmed the expected hexacoordination for this $3d^6$ ion with the oxime as the planar ligand, and chloride and 4-substituted pyridines as axial ligands in the solid state. The ^{1}H-NMR spectra (Fig. 2) also confirmed the presence of 4-substituted pyridines in the Co^{III} state in solution even in the presence of a coordinating solvent such as CD_3CN. In the process of elucidating the nature of the second Co^{III} species observed for **1** during the CV experiment we considered the formation of the homoaxial species $[Co^{III}(prdioxH)(Cl)_2]$ and/or $[Co^{III}(prdioxH)(^{4tBu}py)_2](PF_6)_2$. These species were independently synthesized and their redox behavior was compared, as shown in Fig. 6.

A potential of −0.70 V_{Fc/Fc^+} observed for the second Co^{III}/Co^{II} process of **1** matched the equivalent process in the dichloro analog, thus suggesting its formation during the CV experiment. A similar result was obtained for **3**. On the other hand,

Table 1 Cyclic voltammetric parameters for **1–3** in CH_3CN. Potentials reported *vs.* Fc/Fc^+

	Co^{III}/Co^{II} $E_{1/2}$, $[E_{p,c}; E_{p,a}]$, V (ΔE, V) $\lvert i_{pc}/i_{pa}\rvert$	Co^{II}/Co^{I} $E_{1/2}$, V (ΔE, V) $\lvert i_{pc}/i_{pa}\rvert$	$C{=}N/C^{\bullet}{-}N^-$ $E_{1/2}$, V (ΔE, V) $\lvert i_{pc}/i_{pa}\rvert$	Other L-based events $E_{1/2}$, V (ΔE, V) $\lvert i_{pc}/i_{pa}\rvert$
1	$E_{p,c}$: −0.49; $E_{p,a}$: −0.19 −0.70 (0.10) |0.91|	−1.09 (0.11) |0.99|	−2.11 (0.23) |2.23|	
2	−0.59 (0.12) |0.45|	−1.07 (0.08) |1.09|	−2.07 (0.23) |N/A|	
3	$E_{p,c}$: −0.43; $E_{p,a}$: −0.13 −0.68 (0.11) |1.41|	−1.09 (0.08) |1.19|	−2.22 (0.12) |5.99|	−1.79 (0.08) |N/A| −1.91 (0.03) |1.03|

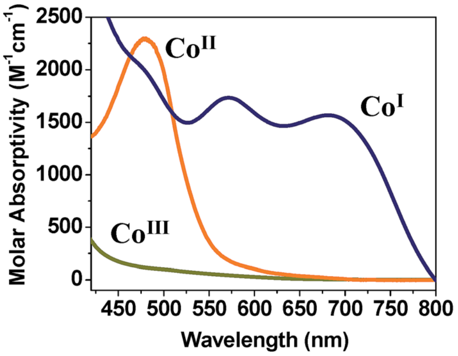

Fig. 5 UV-visible absorption spectra of **1** (Co^{III}) and its reduced Co^{II} analogue with $\lambda = 480$ nm ($\varepsilon = 2288$ M^{-1} cm^{-1}) and Co^{I} analogue with $\lambda = 572$ nm ($\varepsilon = 1738$ M^{-1} cm^{-1}) and $\lambda = 685$ nm ($\varepsilon = 1570$ M^{-1} cm^{-1})].

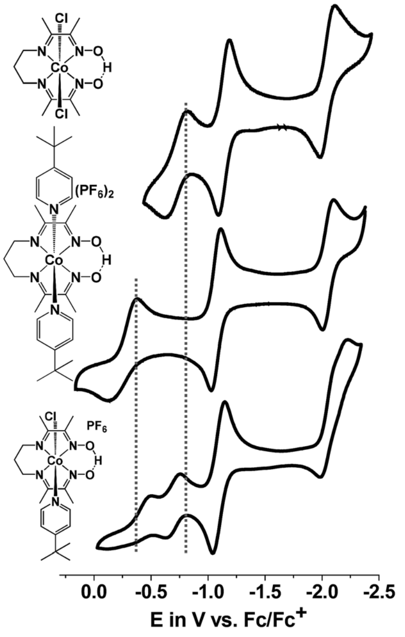

Fig. 6 Comparison of CVs for the heteroaxial **1** (bottom), homoaxial $[Co^{III}(prdioxH)(Cl)_2]$ (top), and homoaxial $[Co^{III}(prdioxH)(^{4tBu}py)_2]PF_6$ (middle), in CH_3CN. The second Co^{III}/Co^{II} event appears at similar potentials for **1** and its dichloro analogue, suggesting the formation of the latter species during the reduction of **1**.

there was considerable mismatch between the cathodic potential for **1** at −0.49 V_{Fc/Fc^+} and the cathodic Co^{III}/Co^{II} potential of the bis-pyridine species at −0.37 V_{Fc/Fc^+}. These combined results are suggestive that the uncoordinated chloride ion is capable of displacing the pyridine coordinated to the Co ion in **1**. However formation of a homoaxial bis-pyridine adduct is highly unlikely. In order to determine whether this substitution is driven by electrochemical reduction[7] or by chemical lability of the axial ligands in the trivalent state of **1**, we performed ^{1}H-NMR experiments in which external sources of chloride or ^{4tBu}pyridine were added. In independent experiments we added 1 equiv. ^{4tBu}pyridine, tetraethylammonium chloride (Et_4NCl) or triethylamine (Et_3N) to the CD_3CN solution of **1** and compared their ^{1}H-NMR spectra with those of **1** and free ^{4tBu}pyridine (Fig. 7a). Note that in these experiments the valence of the Co^{III} ion remained unchanged. Complete spectra are shown in Fig. S13.†

Uncoordinated ^{4tBu}pyridine exhibited two sets of ^{1}H-NMR peaks at 7.36 (H_B) and 8.50 (H'_A) ppm whereas the coordinated ^{4tBu}pyridine in **1** displayed peaks at 7.35 (H_B) and 7.52 (H_A) ppm. The H_B protons retain the same chemical shift but the H'_A protons shifted from 8.50 to 7.52 ppm on coordination of the ^{4tBu}pyridine to the metal center. After 1 equiv. of ^{4tBu}pyridine was added to the CD_3CN solution of **1**, the appearance of signals from the uncoordinated ^{4tBu}pyridine protons at 8.55 ppm (2H) was observed and an increase of the intensity of the peak at 7.37 ppm (2H + 2H) was found whereas the proton count at 7.48 ppm of the coordinated ^{4tBu}pyridine did not change in intensity suggesting no coordination of the external ^{4tBu}pyridine ligand and therefore no replacement of the chloride on cobalt. On the contrary, when 1 equiv. of Et_4NCl (the external chloride source) was added to **1**, peaks at 7.39 (2H) and 8.50 ppm (2H) were found which are characteristic of the uncoordinated ^{4tBu}pyridine ligand. Therefore we conclude that ^{4tBu}pyridine in **1** can be replaced by chloride. This substitution is chemical in nature and the Co ion remains trivalent. The opposite, *i.e.* replacement of chloride by pyridine, is not observed. This substitution pattern was corroborated by DFT calculations[13] *via* comparison of the energetics of the different chemical events. The calculations, reported as free energy changes in kcal mol^{-1}, found the low spin states to be energetically favorable (Table S1†). The low spin state was also confirmed by EPR spectroscopy. The substitution of the ^{4tBu}pyridine ligand by chloride is favorable by *ca.* 10 kcal mol^{-1}, while replacement of chloride by external

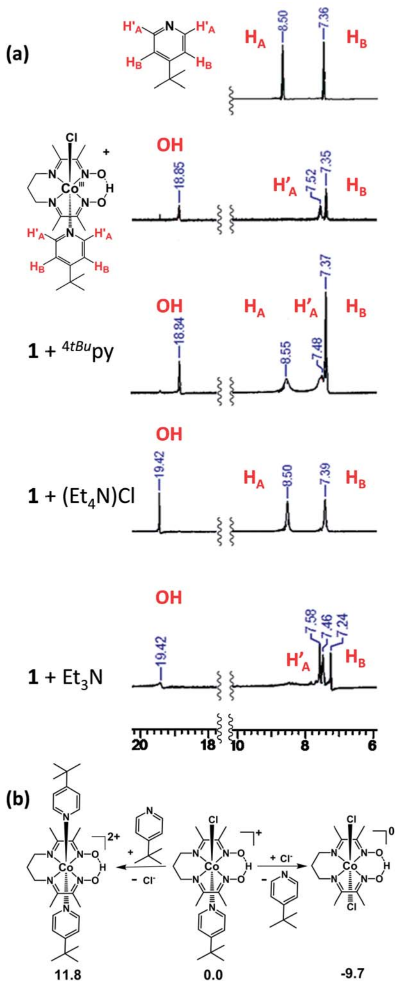

Fig. 7 (a) ^1H-NMR experiments of **1** in CD_3CN upon addition of 1 equiv. of ^{4tBu}pyridine, Et_4NCl, or Et_3N. (b) Energetics of substitution of the axial ligands in **1** as obtained by DFT calculations (energies given in kcal mol^{-1}). As demonstrated by the ^1H-NMR spectra and DFT calculations, chloride can replace the ^{4tBu}pyridine ligand in **1** but the ^{4tBu}pyridine ligand cannot substitute the chloride.

^{4tBu}pyridine is unfavorable by *ca.* 12 kcal mol^{-1} (Fig. 7b). The energetics of pyridine substitution are shown in Table 2 for **1–3** and the proposed mechanism involves an unsaturated five-coordinate intermediate. This event requires *ca.* 14 kcal mol^{-1}, is energetically unfavorable and the limiting step for **1** and **3**. Chloride addition to the five-coordinate intermediate is favored by 23 kcal mol^{-1} and drives the overall ($A + B$) substitution process forward by 9–10 kcal mol^{-1}.

On the other hand, complex **2** with an electron-donating pyrrolidine ligand has the most energy-demanding first step (20 kcal mol^{-1}) and shows little preference for pyridine substitution with a total energy of the substitution process at −3.2 kcal mol^{-1}. This is in agreement with absence of a second Co^{III}/Co^{II} process during the CV experiment. We also probed the acidic nature of the oxime-OH hydrogen as it can contribute to the CV response and found out that no deprotonation, *i.e.* no change of the proton count or shift of the oxime-OH hydrogen at 18.84 ppm was observed upon addition of ^{4tBu}pyridine. On the contrary, when 1 equiv. of Et_3N was added to **1** in CD_3CN, we observed near complete disappearance of the oxime-OH peak intensity and slight shift of the position of the signal from the OH suggesting that Et_3N can deprotonate the ligand. In summary, these results allow us to conclude that the second Co^{III}/Co^{II} redox event observed for **1** and **3** is associated with the chemical formation of $[Co^{III}(prdioxH)(Cl)_2]$. The chemical, rather than electrochemical basis for this process is supported by the fact that external ^{4tBu}pyridine is unable to replace the chloride in the trivalent Co ion nor to deprotonate the oxime –O–H⋯O– moiety. On the other hand, facile replacement of ^{4tBu}pyridine by chloride on Co(III) was observed. This observation of a chemical, rather than electrochemical process diverges from the mechanism proposed by Gerli and Marzilli.[7] Furthermore, the presence of an electron-donating moiety attached to the pyridine strengthens the Py–Co bond and prevents substitution in **2**.

Table 2 Energetics of pyridine substitution by DFT calculations

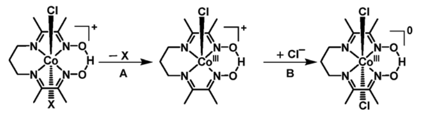

X	A^a	B^a	$(A + B)^a$
^{4tBu}py	13.5	−23.2	−9.7
^{4Pyr}py	20.0	−23.2	−3.7
^{4Bz}py	14.1	−23.2	−9.1

[a] Values in kcal mol^{-1}.

The coordination environment of the Co^{II} species. The nature and spin states of the Co^{II} species generated after the first and second Co^{III} reduction events were interrogated by EPR spectroscopy. Bulk electrolyzed samples of **1** were obtained by the application of appropriate potentials at −0.20 $V_{Ag/AgCl}$ (−0.63 V_{Fc/Fc^+}) for the first or −0.46 $V_{Ag/AgCl}$ for the second Co^{III}/Co^{II} couple. The third reduction event at −0.66 $V_{Ag/AgCl}$ is attributed to formation of a Co^I species. The CW X-band EPR spectra are shown in Fig. 8. The parent complex is EPR silent ($S = 0$), as expected for a low spin Co^{III} species ($^{LS}3d^6$; Fig. 8a). The species resulting from the first redox event (−0.20 $V_{Ag/AgCl}$) is paramagnetic and generates a spectrum (Fig. 8(b1)) with relatively low g-tensor anisotropy and small ^{59}Co hyperfine splitting ($I(^{59}Co) = 7/2$), and resolved superhyperfine structure in the high-field region. The magnetic resonance parameters obtained by simulation of the spectrum (Fig. 8(b2)) are as follows: $g = 2.207, 2.176, 2.015$; $A(^{59}Co) = 65, 80, 260$ MHz; $A(^{14}N) = 36, 39, 48$ (both ^{14}N nuclei). This type of spectrum and these magnetic resonance parameters are in good agreement with previous EPR studies of cobalt oximes ($^{LS}3d^7$, $S = 1/2$) axially coordinated by two nitrogen atoms, which are responsible for the superhyperfine structure.[14] Note, that superhyperfine structure from equatorial nitrogen atoms is here not observed in the EPR spectra, which is typical for cobalt oximes or related complexes, since their hyperfine couplings are much smaller than those of

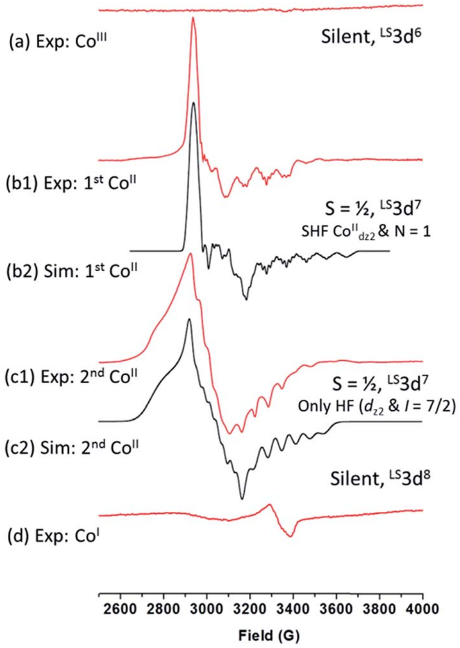

Fig. 8 CW X-band EPR experiments to probe the spin-states and coordination environments of the complexes (Co^{III}, Co^{II}, and Co^{I}) generated during the electrochemistry of **1** in CH_3CN. Spectra (b1) and (c1) were obtained after bulk electrolysis of **1** at −0.20 $V_{Ag/AgCl}$ and −0.46 $V_{Ag/AgCl}$, respectively.

axially coordinated nitrogen atoms.[14,15] These results suggest axial ligation of the central cobalt ion by two nitrogen ($I(^{14}N) = 1$) atoms implying a six-coordinate cobalt center, either with two ^{4tBu}pyridines, one ^{4tBu}pyridine and one CH_3CN, or two CH_3CN moieties.

Based on the EPR data alone it is not possible to pinpoint the nature of these axial ligands, however we rule out the presence of two ^{4tBu}pyridines based on the mismatch of observed redox potentials between **1** and $[Co^{III}(prdioxH)(^{4tBu}py)_2]^{2+}$ in Fig. 6. Furthermore, DFT calculations suggest that formation of a $[Co^{II}(prdioxH)(CH_3CN)_2]^+$ from $[Co^{II}(prdioxH)(CH_3CN)]^+$ is unfavorable by about 9 kcal mol^{-1} in good agreement with results reported by Artero *et al.*[6m] Therefore, we propose that once the chloride is lost, a five-coordinate species $[Co^{II}(prdioxH)(^{4tBu}py)]^+$ is formed as an intermediate. Loss of chloride following the reduction of **1** leads to minor conformational changes, where the Co^{II} ion is displaced by 0.15 Å out of the plane of the macrocyclic ligand and towards the remaining ^{4tBu}pyridine (Fig. 9).

This change likely sterically precludes coordination of a second ^{4tBu}pyridine, but may allow for coordination of a linear CH_3CN molecule. This coordination to $[Co^{II}(prdioxH)(^{4tBu}py)]^+$ species is, in principle, thermodynamically unfavorable in good agreement with the literature.[6m] However it may take place considering the large excess of CH_3CN as solvent. The Co^{II}-species resulting from the second redox event at −0.46 $V_{Ag/AgCl}$ equally supports a $^{LS}3d^7$ center with $S = 1/2$, but with a different *g*-tensor, hyperfine structure, and no superhyperfine splitting (Fig. 8(c1)). The simulation of this spectrum (Fig. 8(c2)) yields the following magnetic resonance parameters: $g = 2.320, 2.200, 2.017$; $A(^{59}Co) = 120, 95, 180$ MHz. These results suggest that axial coordination by nitrogen atoms is unlikely.[14a] Similarly, the magnetic resonance parameters, especially the hyperfine splitting in the high field region due to ^{59}Co, do not support coordination by oxygen, *e.g.*, from adventitious H_2O. We tentatively assign this spectrum to a Co-species with one or two axial chloride ions. Titration experiments were carried out with **1** to evaluate the effects of adding chloride and ^{4tBu}pyridine ligands during the electrochemical experiment (Fig. 10a).

We observed that in presence of increasing amounts of Et_4NCl, the first Co^{III}/Co^{II} process decreases while the second process increases in intensity. While the first process disappeared after *ca.* 0.6 equivalents of Et_4NCl, addition of ^{4tBu}pyridine showed only minor cathodic shifts for both the Co^{III}/Co^{II} processes. The CV (Fig. S5†) of a fresh solution prepared with 1 : 1 Et_4NCl and **1** confirmed the disappearance of the first Co^{III}/Co^{II} process and an increase in intensity of the second process. As expected, both the Co^{III}/Co^{II} processes retained their intensities in a similarly prepared solution of 1 : 1 ^{4tBu}pyridine and **1** (Fig. S5†). These results confirm the CV experiments in Fig. 10a and suggest that the chloride ion is involved in both the Co^{III}/Co^{II} reduction events of complex **1**. On the other hand, ^{4tBu}pyridine has little or no effect on the Co^{III}/Co^{II} reduction. DFT calculations support that loss of chloride after the first Co^{III}/Co^{II} reduction of **1** is thermodynamically favorable by 6.8 kcal mol^{-1} and yields the five-coordinate $[Co^{II}(prdioxH)(^{4tBu}py)]^+$. Alternatively, dissociation of the ^{4tBu}pyridine ligand is calculated to be lower in energy by 10.2 kcal mol^{-1}. These results demonstrate that there is a greater thermodynamic preference of $[Co^{II}(prdioxH)(^{4tBu}py)(Cl)]$ to release ^{4tBu}pyridine rather than chloride giving rise to $[Co^{II}(prdioxH)(Cl)]$. However, calculations of the transition states of the axial ligand dissociation find that loss of chloride is associated with a smaller kinetic barrier than that of the dissociation of ^{4tBu}pyridine (Fig. 10b). The difference between the activation energies is 1.2 kcal mol^{-1}. The Arrhenius model, $k = A\,e^{(-E/RT)}$, estimates that the rate constant k of a chemical reaction increases by 10 times with a decrease of the activation energy E by 1.36 kcal mol^{-1} at 298 K. Therefore, we propose that the dissociation of the axial ligands from $[Co^{II}(prdioxH)(^{4tBu}py)(Cl)]$ is kinetically controlled favoring the formation of $[Co^{II}(prdioxH)(^{4tBu}py)(CH_3CN)]^+$ which is confirmed by EPR as well (Fig. 8). A comparison of X-ray crystal and DFT-calculated

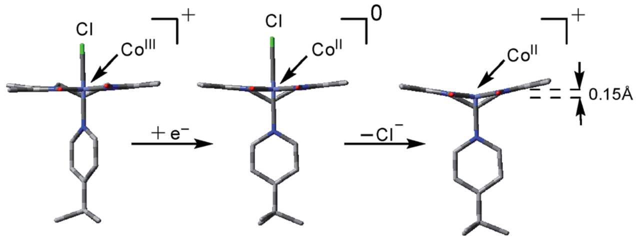

Fig. 9 DFT-optimized geometries of $[Co^{III}(prdioxH)(^{4tBu}py)(Cl)]^+$, $[Co^{II}(prdioxH)(^{4tBu}py)(Cl)]$, and $[Co^{II}(prdioxH)(^{4tBu}py)]^+$. The metal center is displaced by 0.15 Å off of the plane of the macrocyclic oxime ligand in $[Co^{II}(prdioxH)(^{4tBu}py)]^+$.

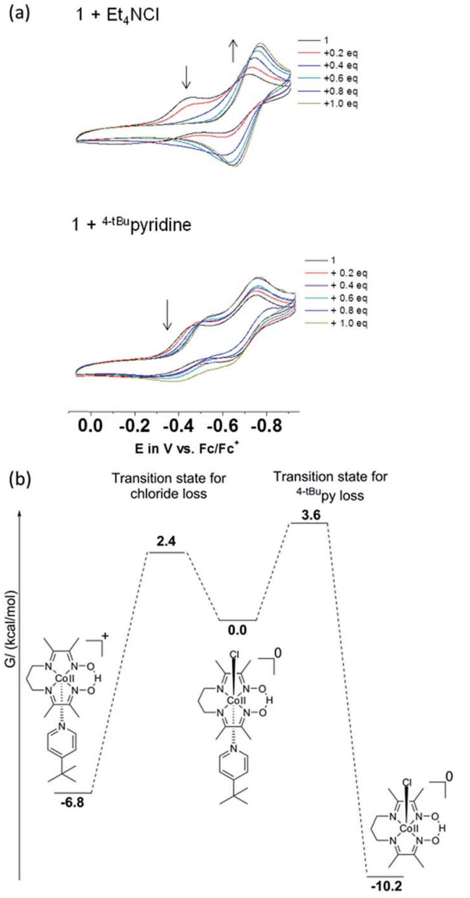

Fig. 10 (a) Changes of the CVs of **1** upon addition of Et_4NCl or ^{4tBu}pyridine in CH_3CN. The first Co^{III}/Co^{II} event gradually disappears with increasing Cl^-, whereas ^{4tBu}Py has no effect. (b) Calculated free energies and activation barriers for **1**. Dissociation of Cl^- is more favorable than that of ^{4tBu}Py yielding $[Co^{III}(prdioxH)(^{4tBu}py)]^+$.

metal–ligand bond distances for **1** is shown in Table 3 along with the DFT bond distances for the $1e^-$ reduced analog of **1**. The Co^{III} reduction is associated with filling of the d_{z^2} orbital which is antibonding in nature. This process increases the bond distance along the *z* axis of the Co^{II} complex facilitating dissociation of the axial ligands. The Co–Cl bond elongates by 0.441 Å, thus considerably more than the 0.300 Å observed for the Co–N5 (^{4tBu}py) bond and becomes more labile so that loss of chloride is invoked upon reduction of **1**. The dichloro analog $[Co^{II}(prdioxH)(Cl)_2]^-$, obtained from the reduction of the *in situ* generated $[Co^{III}(prdioxH)(Cl)_2]$, is negatively charged and chloride loss is expected to be even more favorable. This ligand loss is calculated at 9.7 kcal mol^{-1} and yields the five-coordinate neutral $[Co^{II}(prdioxH)(Cl)]$ species. Uptake of a CH_3CN molecule by the latter species followed by substitution of the remaining chloride by ^{4tBu}pyridine yields $[Co^{II}(prdioxH)(^{4tBu}py)(CH_3CN)]^+$. These events are calculated at 10.0 and 3.6 kcal mol^{-1}, respectively. These substitution processes are thermodynamically less favorable and may be slow, as suggested by the absence of hyperfine structure in the EPR spectrum of the Co^{II}-species obtained after the second Co^{III} reduction of **1**. We conclude that a six-coordinate geometry with ^{4tBu}pyridine as one axial ligand and a CH_3CN ligand as second is favored by the Co^{II} species formed after the first reduction.

A five-coordinate geometry with ^{4tBu}pyridine as the axial ligand maybe present in a certain admixture. Even though the binding of CH_3CN is – according to DFT calculations – energetically not favorable, the large excess of CH_3CN as solvent shifts the equilibrium towards the six-coordinate species. The $3d^7$ Co^{II} species are low-spin. The second reduction involves conversion of $[Co^{III}(prdioxH)(Cl)_2]$ to $[Co^{II}(prdioxH)(Cl)_2]^-$ that yields $[Co^{II}(prdioxH)(Cl)]$ and possibly $[Co^{II}(prdioxH)(CH_3CN)(Cl)]$. In the divalent state chloride is amenable to substitution by ^{4tBu}pyridine ligand thus forming $[Co^{II}(prdioxH)(^{4tBu}py)]^+$ and possibly $[Co^{II}(prdioxH)(^{4tBu}py)(CH_3CN)]^+$. Therefore, prior to the reduction from Co^{II} → Co^{I} a single species $[Co^{II}(prdioxH)(^{4tBu}py)(CH_3CN)]^+$ is present in solution, as evidenced by the presence of a single wave in Fig. 4. Like for the first reduction, the $3d^7$ Co^{II} species are low-spin.

The coordination environment of Co^{I} species. The resulting EPR spectrum of the fraction obtained after bulk electrolysis of **1** at −0.95 $V_{Ag/AgCl}$ in CH_3CN showed only a very weak signal around $g = 2.01$ (Fig. 8d). We propose that this Co^{I} ($^{LS}3d^8$) species is five-coordinate with ^{4tBu}pyridine occupying the axial position of the metal center. This species was also independently obtained by reduction of **1** in dry THF in presence of 2 equiv. of decamethylcobaltocene under an argon atmosphere.[13] The ^{1}H-NMR spectrum of the resulting dark-blue Co^{I} species in CD_3CN is shown in Fig. 11.

Well-defined peaks between 1 and 9 ppm confirmed the low spin nature of the species. Three peaks associated with the aromatic protons of the ^{4tBu}pyridine ligand appear between 7 and 9 ppm. The peaks observed at 7.70 and 7.00 ppm are associated with the H_A and H_B protons of the coordinated ^{4tBu}pyridine, as discussed in Fig. 7. This species is described as $[Co^{I}(prdioxH)(^{4tBu}py)]$ (**4**). Five-coordinate Co^{I} complexes similar to **4** have been reported.[8,9,16]

While running the previous NMR experiments we were able to grow crystals from the deuterated solvent and solve the structure of a dimeric product in Fig. 12. The structure confirms the presence of an apical pyridine on the catalytically active Co^{I} species thus validating the proposed mechanism beyond reasonable doubt. In the time scale of the cyclic voltammetric and electrocatalytic experiment, this species is clearly monomeric, suggesting that the observed dimer is the result of a kinetically sluggish reaction. Dimer formation resulting from reduction with cobaltocene derivatives has been observed in related oxime species[17] and might point out to possible deactivation pathways for the catalyst.

In light of the comprehensive UV-visible, EPR, NMR, and DFT data accumulated in our study, we propose a viable chemical and electrochemical pathway starting from the parent **1** and reducing to the Co^{II} counterpart and to the catalytically active monovalent species (Scheme 1). The first Co^{III}/Co^{II} reduction shown in step 1 is followed by loss of a chloride to yield the five-coordinate Co^{II} species $[Co^{II}(prdioxH)(^{4tBu}py)]^+$. The latter species incorporates a CH_3CN molecule to form the six-coordinate Co^{II} complex $[Co^{II}(prdioxH)(^{4tBu}py)(CH_3CN)]^+$

Table 3 Co–ligand bond lengths[a] of **1** from X-ray crystal and DFT-optimized structures. Metal–ligand bond distances[a] of the one-electron reduced (Co^{II}) analog of **1** are also reported

		$Co–N_1$	$Co–N_2$	$Co–N_3$	$Co–N_4$	$Co–N_5$	Co–Cl
Experiment	$[Co^{III}(prdioxH)(^{4tBu}py)(Cl)]^+$	1.903	1.917	1.914	1.898	1.975	2.237
Theory	$[Co^{III}(prdioxH)(^{4tBu}py)(Cl)]^+$	1.907	1.925	1.928	1.905	1.988	2.304
Theory	$[Co^{II}(prdioxH)(^{4tBu}py)(Cl)]$	1.904	1.927	1.928	1.904	2.288	2.745

[a] Values are in Å.

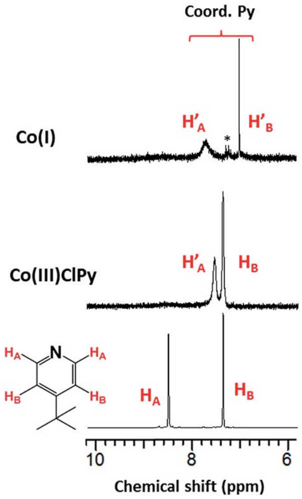

Fig. 11 ^1H-NMR spectra of $[Co^I(prdioxH)(^{4tBu}py)]$, in CD_3CN. The asterisk denotes the presence of adventitious toluene. See ESI† for the complete spectra.

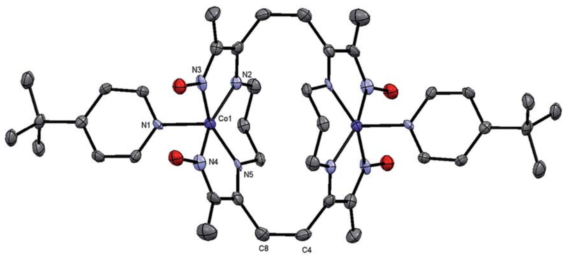

Fig. 12 ORTEP representation of the crystal structure for the neutral dimer of **4** (CCDC 1448834) at 50% ellipsoid probability. Hydrogen atoms omitted for clarity. Co(1)–N(1) = 1.997(4); Co(1)–N(2) = 1.902(4); Co(1)–N(3) = 1.866(4); Co(1)–N(4): 1.850(4); Co(1)–N(5) = 1.890(4); C(4)–C(8) = 1.592(6).

described in step 2. The released chloride in step 1 replaces the ^{4tBu}pyridine in the remaining $[Co^{III}(prdioxH)(^{4tBu}py)(Cl)]^+$ (**1**) as observed generating a second six-coordinate Co^{III} species with two chlorides occupying the axial positions, step 3, along with uncoordinated ^{4tBu}pyridine. This is a chemical, rather than electrochemical step. The second Co^{III}/Co^{II} reduction, shown in step 4, yields the six-coordinate $[Co^{II}(prdioxH)(Cl)_2]^-$ that is subsequently converted into the five-coordinate $[Co^{II}(prdioxH)Cl]$. Uptake of a solvent CH_3CN molecule by the latter species (step 5) may take place and is followed by replacement of the remaining chloride with one ^{4tBu}pyridine present in solution to give rise to the species $[Co^{II}(prdioxH)(^{4tBu}py)(CH_3CN)]^+$ in step 6. This species is then reduced and transforms into the five-coordinate and catalytically active $[Co^I(prdioxH)(^{4tBu}py)]$ with release of the CH_3CN molecule in step 7. It is important to mention that Marzilli[7] proposed generation of a Co^{II}–Cl species already in step 1. It was further proposed that an outer sphere electron transfer mechanism involving the newly generated Co^{II}–Cl species and the parent Co^{III} complex, and chloride transfer from one metal center to another could yield a Co^{III} dichloro species. The chloride transfer event is calculated to be favorable by 6.7 kcal mol^{-1}. The present study offers an alternative pathway where the Co^{III} dichloro species is generated *via* substitution of ^{4tBu}py already on the parent Co^{III} complex by an external chloride, this process being favorable by 9.7 kcal mol^{-1}.

Catalytic activity and proposed mechanisms

The optimization of proton-reducing catalysts requires a detailed study of catalytic parameters such as overpotentials (η), turnover numbers (TON), and faradaic efficiencies (% FE) allied to an understanding of the plausible catalytic mechanisms. In the next paragraphs we discuss the experimental and theoretical results observed for complexes **1–3**.

Catalytic profiles and yields. We investigated the electrocatalytic behavior of **1** in the presence of trifluoroacetic acid (HTFA, $pK_a = 12.7$ in CH_3CN), and the CV data revealed a catalytic peak appearing near the reduction potential of the Co^{II}/Co^I couple upon incremental addition of 0–10 equiv. of HTFA (Fig. 13). The results confirm the Co^I species as catalytically active, and generation of H_2 happens at the low overpotential of 0.35 V measured including the homoconjugation effect of the acid.[18] The CV profile of the Co^{III}/Co^{II} couple did not change with increasing amounts of acid, ruling out the possibility of the involvement of this couple towards proton reduction. We also observed a new process appearing at a slightly more negative potential than that of the catalytic peak in the presence of ≥5 equiv. of HTFA and tentatively attributed to the $Co^{III}–H^-/Co^{II}–H^-$ couple. This attribution is supported by DFT calculations. The reduced analog for **1** was generated *via* controlled potential electrolysis at $-1.0\ V_{Ag/AgCl}$ in the presence of HTFA and TONs were determined by gas-chromatography. A TON of 18.7 (*ca.* 40% conversion ratio) was observed after 3 h in CH_3CN in presence of 4.0×10^{-5} mol of **1** and 100 equiv. of HTFA with % FE ≈ 80%. This solution displayed a color change from light yellow, typical of the Co^{III} parent species, to dark green during

Step 1. $[Co^{III}(prdioxH)(^{4tBu}py)(Cl)]^{+} + e^{-} \rightarrow [Co^{II}(prdioxH)(^{4tBu}py)(Cl)]^{o} \rightarrow [Co^{II}(prdioxH)(^{4tBu}py)]^{+} + Cl^{-}$
Step 2. $[Co^{II}(prdioxH)(^{4tBu}py)]^{+} + CH_3CN \rightarrow [Co^{II}(prdioxH)(^{4tBu}py)(CH_3CN)]^{+}$
Step 3. $[Co^{III}(prdioxH)(^{4tBu}py)(Cl)]^{+} + Cl^{-} \rightarrow [Co^{III}(prdioxH)(Cl)_2]^{o} + {}^{4tBu}py$
Step 4. $[Co^{III}(prdioxH)(Cl)_2]^{o} + e^{-} \rightarrow [Co^{II}(prdioxH)(Cl)_2]^{-} \rightarrow [Co^{II}(prdioxH)(Cl)]^{o} + Cl^{-}$
Step 5. $[Co^{II}(prdioxH)(Cl)]^{o} + CH_3CN \rightarrow [Co^{II}(prdioxH)(CH_3CN)(Cl)]^{o}$
Step 6. $[Co^{II}(prdioxH)(CH_3CN)(Cl)]^{o} + {}^{4tBu}py \rightarrow [Co^{II}(prdioxH)(^{4tBu}py)(CH_3CN)]^{+} + Cl^{-}$
Step 7. $[Co^{II}(prdioxH)(^{4tBu}py)(CH_3CN)]^{+} + e^{-} \rightarrow [Co^{I}(prdioxH)(^{4tBu}py)]^{o} + CH_3CN$

Scheme 1 Proposed chemical and electrochemical pathway from **1** the catalytically active Co^{I} species.

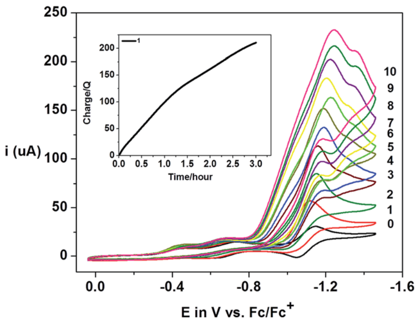

Fig. 13 CV experiments showing the electrocatalytic behavior of **1** towards H_2 generation in the presence of HTFA in CH_3CN solution. The numbers 0–10 indicate the number of equiv. of HTFA. (Inset) Plot of charge consumed against time during the bulk-electrolysis experiment for dihydrogen generation by **1** after 3 h.

the controlled potential electrolysis experiment. Complex **1** consumed *ca.* 200 C of charge over 3 h (Fig. 13, inset) validating its catalytic activity. Electrocatalytic H_2 generation was also confirmed for **2** and **3** (Fig. S6 and S7†) following similar methodology. Overpotentials for **1–3** were calculated from CV experiments whereas TONs and % FEs were measured from controlled potential electrolysis and are reported in Table 4. All species exhibited low overpotential, higher charge consumption, and catalytic current with respect to the blank (Fig. S8–S10†). These results suggest that although variation of the substituents on the pyridine ligand has a minor effect on the overpotential of **1–3**, the TONs showed considerable differences. Complex **1** with an electron-donating group displayed the highest catalytic activity. The % FE for proton reduction was calculated to be *ca.* 80%, thus suggesting the possible conversion of the catalyst into non-catalytic species. Indeed, calculations found some degree of redox non-innocence in the ligand during the reduction event (Fig. S11, Table S2†) suggesting the possibility of a $3d^8/3d^7$-$L^{\bullet}$ equilibrium between $[Co^{I}(prdioxH)(^{4tBu}py)]$ and $[Co^{II}(prdioxH^{\bullet})(^{4tBu}py)]$. However the $3d^7$-$L^{\bullet}$ species would be strongly antiferromagnetically coupled yielding an overall singlet ($S = 0$) state not observable by EPR spectroscopy.

Table 4 Catalytic parameters for **1–3** in CH_3CN in the presence of HTFA at a catalyst-to-acid ratio of 1 : 100

Catalytic parameters	1	2	3
$E(H^+/H_2)$ (V) *vs.* Fc/Fc$^+$	−1.03	−1.04	−1.03
Overpotential (V) (10 eq. HTFA)	0.35	0.36	0.35
TON/3 h (4.0×10^{-5} mol)	18.7	13.8	13.8
Faradaic efficiency (%)	77	84	75

Catalytic pathways for H_2 evolution. Previous studies[6a,c,d,f,g,i,k,m,10g] on hydrogen evolution by cobalt oximes propose the formation of a Co^{III}–H^- hydride intermediate, either by heterolytic $[LCo^{II}$–$H^-] + H^+ \rightarrow [LCo^{II}] + H_2$ or by bimolecular homolytic $2[LCo^{II}$–$H^-] \rightarrow 2[LCo^{I}] + H_2$ pathways. The chosen pathway depends on the strength of the acid used as proton source in the organic medium.[3e] Proton-coupled electron transfer (PCET) may become relevant in sufficiently acidic systems. Theoretical results[6i,f,g] support the formation of a Co^{III}–H^- intermediate from protonation of the Co^{I} complex as the most likely mechanism. A $1e^-$ reduction of the Co^{III}–H^- species generates the Co^{II}–H^- intermediate which reacts heterolytically with a proton to produce H_2. However if the $E_{(Co^{III}–H^-/Co^{II}–H^-)}$ potential for Co^{II}–H^- generation is more negative than $E_{(Co^{II}/Co^{I})}$, intermediacy of a Co^{II}–H^- species is unlikely and H_2 evolution will likely be realized from protonation of the Co^{III}–H^- species in a heterolytic manner. Support for a bimolecular homolytic mechanism has been reported,[9] albeit without strong kinetic evidence. The formation of a transient Co^{III}–H^- complex has been reported[4b] from the protonation of a $[Co^{I}(triphos)(CH_3CN)]PF_6$ (triphos = 1,1,1-tris(diphenylphosphinomethyl) ethane) species and both the heterolytic and homolytic pathways were invoked for H_2 generation. Protonation at the oxime bridge (O–H⋯O) of the Co^{II} species is only possible in presence of a sufficiently strong acid with a $pK_a \leq 10.7$ in CH_3CN.[6f]

In presence of *p*-cyanoanilinium (pK_a 7.6 in CH_3CN), the electrocatalytic wave of a cobalt oxime complex was observed at a potential of 320 mV more positive than that required for the Co^{II}/Co^{I} reduction[6m] and a pathway involving the protonation of the oxime bridge was proposed to explain the observed potential shift. Although the thermodynamics of these pathways have been studied in reasonable detail, the free energy barriers for the proton transfer and H_2 production steps are considerably less understood.

Recent studies consider the protonation of the glyoxime bridge by a Co^{III}–H^- moiety[19] or even the lack of formation of Co^{III}–H^-.[17] Although potentially relevant—especially to evaluate catalyst decomposition mechanisms—these pathways will require further validation and for the purposes of this study we will assume the need for formation of the Co^{III}–H^- hydride intermediate. The protonation of the oxime bridge in

$[Co^{II}(prdioxH)(^{4tBu}py)]^+$ species seems energetically unfavorable by 19 kcal mol^{-1}. This is consistent with a previous study where it was proposed that the weak acid HTFA cannot protonate the oxime moiety.[6f]

Complexes **1–3** displayed electrocatalytic waves in the presence of 10 equiv. HTFA at potentials close to the reduction of Co^{II}/Co^{I}. The respective $E_{1/2}^{(H^+/H_2)}$ are −1.03, −1.04 and −1.03 V_{Fc/Fc^+} and the Co^{II}/Co^{I} reduction potentials are −1.09, −1.07 and −1.09 V_{Fc/Fc^+} for **1**, **2**, and **3**, respectively. The catalytic pathway calculated for **1** is shown in Fig. 14. The calculated potential for the Co^{II}/Co^{I} reduction of **1** is −0.93 V_{Fc/Fc^+} and the species obtained after reduction, $[Co^{I}(prdioxH)(^{4tBu}py)]$, is neutral and can easily take up a proton upon reaction with HTFA. This cobalt protonation is favorable by 8.4 kcal mol^{-1} and yields the cobalt-hydride species described as $[Co^{III}(H^-)(prdioxH)(^{4tBu}py)]^+$. This is expected because Co^{I} is a closed-shell $3d^8$ center and can behave as a good Lewis base.

The reduction potential for the generation of a $Co^{II}–H^-$ from $Co^{III}–H^-$ is −1.43 V_{Fc/Fc^+} and it is in agreement with the appearance of a shoulder at about −1.40 V_{Fc/Fc^+} at higher concentrations of acid in Fig. 13. This potential is more negative than that of the Co^{II}/Co^{I} couple of −0.93 V_{Fc/Fc^+}. Similarly, a PCET event for conversion of the Co^{I} complex into the $Co^{II}–H^-$ species is calculated to be −1.39 V_{Fc/Fc^+}. Because electrocatalysis occurs near the measured value of $E_{(Co^{II}/Co^{I})}$ (Fig. 13), the involvement of a $Co^{II}–H^-$ species is not invoked in the catalytic mechanism. The electrocatalytic wave did not show an anodic shift with the decrease of pH, when compared to the reduction potential of the Co^{II}/Co^{I} couple (Fig. 13) and therefore, a PCET mechanism from the Co^{II} complex, $[Co^{II}(prdioxH)(^{4tBu}py)(CH_3CN)]^+$, to the $Co^{III}–H^-$ species is not considered. The protonation of the latter $Co^{III}–H^-$ species by HTFA leads to the generation of H_2. This event is calculated to be slightly uphill by 2.2 kcal mol^{-1} and is facilitated by the excess of acid present. The Co^{III} complex obtained after the evolution of H_2 contains a trifluoroacetate ligand bound to the metal center.[6l] The reduction of this species is calculated at −0.01 V_{Fc/Fc^+} and yields the corresponding Co^{II} complex, $[Co^{II}(prdioxH)(^{4tBu}py)(TFA)]$, which can exchange the trifluoroacetate ligand by a CH_3CN molecule, reentering the catalytic cycle. This ligand exchange event is nearly isoenergetic at about 1 kcal mol^{-1} and is expected to be favored by the large concentration of the solvent.

The bimolecular mechanism involving two $[Co^{III}(H^-)(prdioxH)(^{4tBu}py)]^+$ complexes can generate H_2 favorably at −28.3 kcal mol^{-1}. However, this pathway may have a moderate kinetic barrier arising from the electrostatic repulsion between two cationic species and is likely plausible at lower concentrations of acid. It is also noteworthy that the complex $[Co^{I}(prdioxH)(^{4tBu}py)]$ obtained after the reduction of $[Co^{II}(prdioxH)(^{4tBu}py)(CH_3CN)]^+$ can undergo an intramolecular electron transfer from metal to the oxime ligand framework giving rise to a radical-containing $[Co^{II}(prdioxH^{\bullet})(^{4tBu}py)]$. Similar to other pathways[17,19] where the ligand is involved, the latter species may contribute to catalyst decomposition. A detailed study about the role of this species is currently underway.

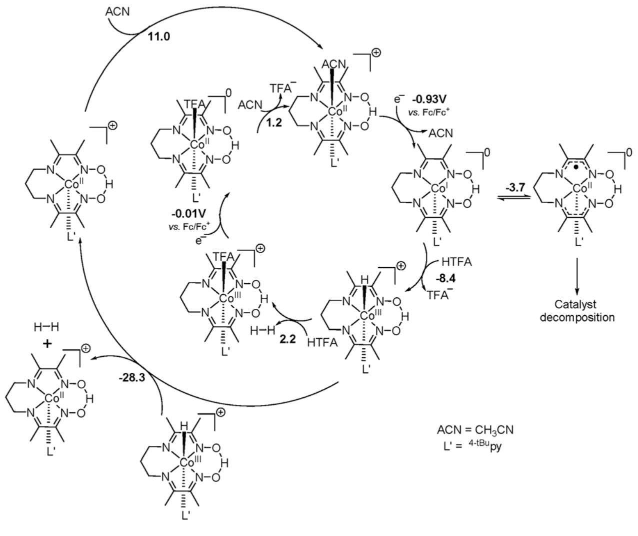

Fig. 14 The catalytic pathways calculated for H_2 evolution by **1** in the presence of HTFA in CH_3CN (ACN). The formation of a $Co^{III}–H^-$ species is invoked. This complex can react either heterolytically with a proton or homolytically with another $Co^{III}–H^-$ complex to yield H_2. The heterolytic pathway involves an acetate-bound Co complex. The homolytic mechanism is more likely at low concentrations of acid. Energies given in kcal mol^{-1} as calculated at the B3PW91//TZVP/6-311++G(d,p) level of theory.

Conclusions

A series of heteroaxial complexes in a trivalent cobalt/oxime macrocyclic framework was synthesized and characterized by multiple physico-chemical techniques. The electrochemistry of these species exhibited complex behavior with two Co^{III}/Co^{II} and one Co^{II}/Co^{I} processes; the origin of which has been identified with multiple redox and spectroscopic methods like CV, ^{1}H-NMR, UV-vis, EPR, and DFT calculations. A detailed understanding of the chemical and electrochemical pathways with distinct coordination preferences was revealed: (i) the first Co^{III}/Co^{II} reduction involves chloride loss followed by incorporation of CH_3CN to form a six-coordinate Co^{II} complex; (ii) the free chloride replaces ^{4tBu}pyridine in the remaining unreduced **1**, and forms a second Co^{III} species with chlorides occupying the axial positions; (iii) this complex is then reduced and yields a five-coordinate Co^{II} species that accommodates a solvent molecule at its sixth axial position; (iv) available ^{4tBu}pyridine replaces the remaining chloride; (v) the resulting species is then reduced, transforming into the five-coordinate and catalytically active $[Co^{I}(prdioxH)(^{4tBu}py)]$. The complexes exhibited catalytic properties towards proton reduction in HTFA/CH_3CN with low overpotentials and good turnover numbers. Variation of the substituent groups in the pyridine ligand affected the final TONs; however overpotentials remained relatively unchanged. A detailed catalytic mechanism favors a heterolytic pathway for hydrogen generation, and involves: (i) a favorable Co^{I} protonation that yields the required $Co^{III}–H^-$ species; (ii) this complex reacting heterolytically with an available proton from HTFA, generating H_2, and therefore regenerating Co^{III}; (iii) this Co^{III} species first incorporating TFA and undergoing reduction followed by CH_3CN exchange prior to reentering the catalytic cycle. Bimolecular mechanisms seem favorable only at lower acid concentrations, and both the $Co^{II}/Co^{III}–H^-$ and $Co^I/Co^{II}–H^-$ PCET events seem unlikely. These results allow for some generalizations on the behavior of heteroaxial cobalt macrocycles and serve as guidelines for the development of new catalysts based on macrocyclic frameworks.

Materials, methods and synthetic procedures

General

Reagents and solvents were used as received from commercial sources. Infrared spectra were recorded from 4000 to 650 cm^{-1} as KBr pellets on a Bruker Tensor 27 FTIR spectrophotometer. ^1H-NMR spectroscopy was carried out with a Mercury FT-NMR 400 MHz setup using CD_3CN as solvent at 25 °C. Chemical shifts are plotted *vs.* TMS. ESI-(+) mass spectrometry was measured in a triple quadrupole Micromass Quattro LC equipment where experimental mass patterns were fitted with the theoretical isotopic distribution. Elemental analysis (C, H, and N) was performed using an Exeter analytical CHN analyzer by Midwest Microlab, an independent lab located in Indianapolis, Indiana, USA. UV-visible spectra were obtained using quartz cells at room temperature in a Varian Cary 50 spectrophotometer operating in the range of 200 to 1000 nm. Values of ε are given in M^{-1} cm^{-1}. HPLC-grade CH_3CN solutions were used for cyclic voltammetry and UV-absorption spectroscopy studies.

Electrochemistry and bulk electrolysis

The electrochemical behavior of complexes **1–3** was investigated with a BAS 50W potentiostat/galvanostat. Cyclic voltammograms were obtained at room temperature in CH_3CN solutions containing 0.1 M of *n*-Bu_4NPF_6 as the supporting electrolyte under an argon atmosphere. The electrochemical cell was comprised of three electrodes: glassy-carbon (working), platinum wire (auxiliary) and Ag/AgCl (reference). The ferrocene/ferrocenium redox couple Fc/Fc^+ ($E^o = 400$ mV *vs.* NHE)[20] was used as the internal standard. Peak to peak potential separation ($\Delta E_p = |E_{p,c} - E_{p,a}|$) and $|i_{pa}/i_{pc}|$ values were measured to evaluate the reversibility of the redox processes. Bulk electrolysis was performed in a custom-made air-tight H-type cell with vitreous carbon as the working electrode, Ag/AgCl as the reference electrode placed in the same compartment and a Pt-coil used as the auxiliary electrode placed in another compartment separated by a frit. Controlled potential electrolysis of the complex has been done in 20 mL CH_3CN with tetrabutyl ammonium hexafluorophosphate ($TBAPF_6$) as supporting electrolyte until the calculated final charge is attained. Potentials were applied to the cell by a BAS 50W potentiostat/galvanostat and measured against the Ag/AgCl reference electrode.

X-ray structural determination

For complex **1** an orange needle-shaped crystal with dimensions 0.40 × 0.16 × 0.11 mm was mounted on a Nylon loop using a small amount of paratone oil. Data were collected in a Bruker CCD (charge coupled device) based diffractometer equipped with an Oxford Cryostream low-temperature apparatus operating at 173 K. Data were measured using omega and phi scans of 0.5° per frame for 30 s. The total number of images was based on results from the program COSMO V1.58 (ref. 21*a*) where redundancy was expected to be 4.0 and completeness to 0.83 Å to 100%. Cell parameters were retrieved using APEX II software[21b] and refined using the SAINT software[21c] for all observed reflections. Data reduction was performed using SAINT which corrects for Lp. Scaling and absorption corrections were applied using the SADABS[21d] multi-scan technique, supplied by George Sheldrick. The structure was solved by the direct method using the SHELXS-97 program and refined by the least squares method on F^2, SHELXL-97, which is incorporated in SHELXTL-PC V 6.10.[21e] The structure was solved in the space group $I\bar{4}$ (# 82). All the non-hydrogen atoms are refined anisotropically. Hydrogens were calculated by geometrical methods and refined as a riding model. Solvent molecules were found to reside in the lattice void, which is presumably octane resulting from crystallization. Attempts to model these solvents and/or to redefine as CH_2Cl_2 failed to generate a chemically sensible model. The SQUEEZE (P. V. D. Sluis & Spek, 1990)[21f] function of PLATON (Spek, 2003)[21g] was used to eliminate the contribution of the electron density in the void from the intensity data. The total solvent area volume was found to be 625 $Å^3$, with electron count of about 80 electrons. This corresponds to approximately two molecules of CH_2Cl_2 residing in the cell. The calculated *F*(000) and density were obtained for the cell containing two molecules of CH_2Cl_2 per cell or one per molecule of interest. The refinement was carried out on the new reflection file generated by PLATON. The crystal used for the diffraction study showed no decomposition during data collection. All the drawings are done at 50% ellipsoids. In the case of complex **3**, a yellow plate-shaped crystal with dimensions 0.16 × 0.10 × 0.04 mm was mounted on a Nylon loop using a small amount of paratone oil. Data were collected using a Bruker CCD (charge coupled device) based diffractometer equipped with an Oxford Cryostream low-temperature apparatus operating at 173 K. Data were measured using omega and phi scans of 0.5° per frame for 30 s. The total number of images was based on results from the program COSMO V1.61 (ref. 21*h*) where redundancy was expected to be 4.0 and completeness to 0.83 Å to 100%. Cell parameters were retrieved using APEX II software[21i] and refined using SAINT for all observed reflections. Data reduction was performed using the SAINT software.[21j] Scaling and absorption corrections were applied using the SADABS[21d] multi-scan technique. The structure was solved by the direct method using the SHELXS-97 program and refined by the least squares method on F^2, SHELXL-97,[21e] which is incorporated in OLEX2.[21k] The structure was solved in the space group $P2_1/c$ (# 14). All the non-hydrogen atoms are refined anisotropically. Hydrogens were calculated by geometrical methods and refined as a riding model. All the drawings are done at 50% ellipsoids.

In the case of complex **4**, blue needle-shaped crystals were grown *via* slow evaporation from deuterated acetonitrile. A single weakly diffracting crystal with dimensions 0.05 × 0.08 × 0.13 mm was mounted on a Nylon loop using a small amount of paratone oil. Data were collected using a Bruker CCD (charge coupled device) based diffractometer equipped with an Oxford Cryostream low-temperature apparatus operating at 100 K. Data were measured using omega and phi scans of 0.5° per frame for 90 s. Cell parameters were retrieved using APEX II software[21i] and refined using SAINT for all observed reflections. Data reduction was performed using the SAINT software.[21j] Scaling and absorption corrections were applied using SADABS21d multi-scan technique. The structure was solved by the direct method using the SHELXS-97 program and refined by the least squares method on F^2, SHELXL-97,[21e] which is incorporated in OLEX2.[21k] The structure was solved in the space group *C*2/*c*. All the non-hydrogen atoms are refined anisotropically. Hydrogens were calculated by geometrical methods and refined as a riding model. All the drawings are done at 50% ellipsoids. We present this structure as a dimer molecule with a C8–C4 bond distance of 1.592 through symmetry of the unit cell. Although we are confident that our interpretation is correct, analysis of the raw data suggests that the crystal chosen is of a multiple nature with more than 3 domains, which may indeed mean that we have not correctly identified the correct unit cell. Use of different indexing programs, and thresholding levels along with viewing the data with a reciprocal viewer program provides us with what we present here as the most reasonable unit cell.

EPR spectroscopy

Continuous wave (CW) X-band (9–10 GHz) EPR experiments were carried out with a Bruker ELEXSYS E580 EPR spectrometer (Bruker Biospin, Rheinstetten, Germany), equipped with a TE_{102} rectangular EPR resonator (Bruker ER 4102st) and a helium gas-flow cryostat (ICE Oxford, UK). An intelligent temperature controller (ITC503) from Oxford Instruments, UK, was used. Data processing was done using Xepr (Bruker BioSpin, Rheinstetten) and Matlab 7.11.1 (the MathWorks, Inc., Natick) environment. Simulations were performed using the EasySpin software package (version 4.5.5) (Stoll & Schweiger, *J. Magn. Reson.*, 2006).

Computational methods

Calculations were performed with a development version of the Gaussian suite of programs,[22a] using B3PW91 (ref. 22*b*–*d*) functional with double-zeta SDD basis set on cobalt and D95 (ref. 22*e* and *f*) basis on the other atoms. All optimized structures were confirmed as minima by analyzing the harmonic vibrational frequencies. Solvation effects in CH_3CN were estimated using the IEF polarizable continuum model (PCM)[22g–j] and were included during structure optimization. Single-point energies were reevaluated with triple-zeta TZVP basis[22k] on the metal atom and 6-311++G(d,p) basis[22l] on the other atoms in presence of the continuum solvation model. The free energies were calculated using the triple-zeta SCF energy while the zero-point energy and thermal corrections were included from the double-zeta calculations. The standard states of 1 M concentration were considered for all the reactants and products for calculating the free energies of reactions. Low-spin configurations yielded lower energies for all the species. The wave functions of the optimized structures were tested for SCF stability.[22m–o] Isosurface plots of orbitals and spin densities were visualized using GaussView.[22p] The calculation of the reduction potentials of the complexes included zero-point energy and thermal corrections and standard thermodynamic equation $\Delta G = -nFE$ was used. The calculated potentials were referenced to a value of $E_{1/2} = 4.678$ V for the ferrocene/ferrocenium couple calculated under our level of theory.

Catalytic activity

Proton reduction electrocatalysis was evaluated for **1–3** by cyclic voltammetry in the presence of trifluoroacetic acid (HTFA) using a glassy carbon as working electrode, platinum wire as auxiliary and Ag/AgCl as reference electrodes with tetra-butyl ammonium tetrafluoroborate ($TBABF_4$) as supporting electrolyte. Overpotential (η), i_c/i_p, and kinetic rate constant, k_{obs}, have been calculated from the observed changes in the voltammogram. To determine the amount of dihydrogen release, bulk electrolysis has been performed in a custom-made air-tight H-type cell in the presence of a mercury-pool as working electrode, Ag/AgCl as reference electrode placed in the same compartment whereas Pt-coil used as the auxiliary electrode placed in the other compartment separated by a frit. $TBABF_4$ was used as the supporting electrolyte. The main chamber was filled with an electrolyte solution and proton source ($TBABF_4$: 1.317 g; TFA: 0.456 g [4 mmol], 20 mL CH_3CN) and the glass-fitted chamber was filled with another electrolyte solution ($TBABF_4$: 0.329 g; 5 mL CH_3CN). In a standard experiment, the cell was purged with N_2 gas for 20 minutes followed by sample head space gas (100 μL) to ensure O_2-free environment in the gas chromatograph (GC). The solution was electrolyzed in the absence of the catalyst for 180 minutes at −1.0 V *vs.* Ag/AgCl. The head space gas was again injected into the GC and the amount of dihydrogen was recorded. Then, the cell was purged with N_2 gas for another 20 minutes followed by injection of the catalyst (0.04 mmol) dissolved in CH_3CN. Bulk electrolysis was conducted for another 180 minutes and the head space gas (100 μL) was injected into the GC to record the amount of dihydrogen produced. After the background subtraction, the turnover number was calculated as the ratio of the moles of dihydrogen produced over the moles of catalyst used. Faradaic efficiency was calculated from the gas chromatography measurements using the equation $\%\ FE = [(n_{H_2})/(Q/2)] \times 100$, where Q is in Faraday unit. The GC is a Gow-Mac 400 instrument equipped with a thermal conductivity detector. An 8′ × 1/8″ long 5 Å molecular sieve column operating at 60 °C was used with the carrier gas N_2. The calibration was carried out with dihydrogen gas (dihydrogen GC grade 99.99%, Scotty analyzed gases, Sigma Aldrich).

Synthetic procedures

The synthesis of the oxime ligand, $prdioxH_2$,[11] and the precursor $[Co^{III}(prdioxH)(Cl)_2]$,[12] followed the literature procedure. The complex $[Co^{III}(prdioxH)(^{4tBu}py)_2](PF_6)_2$ used for electrochemical comparisons was obtained by modifications to the literature procedure[7] and described in Scheme S1.† The synthetic procedure and characterization of $[\mathrm{Co^{III}(prdioxH)(Cl)_2}]$ are described in Scheme S2.†

$[\mathrm{Co^{III}(prdioxH)(^{4tBu}py)(Cl)}]\mathrm{PF_6}$ (1). $[\mathrm{Co^{III}(prdioxH)(Cl)_2}]$ (1 mmol, 0.369 g) was dissolved in 20 mL methanol. A solution of $\mathrm{KPF_6}$ (1.7 mmol, 0.3128 g) in 5 mL water was added to the solution followed by ^{4tBu}pyridine (1 mmol, 0.135 g) in 5 mL of methanol. The reaction mixture was stirred for 2 h and then rotary-evaporated to 10 mL. This solution was kept in storage for 3 days when brownish-yellow crystals were obtained. X-ray quality crystals were obtained after recrystallization from acetone/water (1 : 1) mixture. Yield: 75%. IR (KBr, $\mathrm{cm^{-1}}$) 3645 (w) (OH); 3234 (w) (aromatic-CH); 2969 (s), 2907 (m), 2871 (m) (aliphatic CH); 1620 (s) (C=N); 1432 (m) (C=C); 847 (s) ($\mathrm{PF_6^-}$). ^{1}H-NMR [400 MHz, $\mathrm{CD_3CN}$, 300 K] δ/ppm = 1.249 [s, 9H (*t*-butyl)]; 2.534 [s, 6H ($\mathrm{CH_3}$)]; 2.631 [s, 6H ($\mathrm{CH_3}$)]; 4.173 [m, 4H ($\mathrm{CH_2}$)]; 7.358 [d, 2H (aryl)]; 7.526 [d, 2H (aryl)]. ESI pos. in MeOH: m/z = 468.1573 for $[\mathrm{Co^{III}(prdioxH)(^{4tBu}py)(Cl)}]^+$. Anal. calcd for $\mathrm{C_{20}H_{32}ClCoF_6N_5O_2P}$: C: 39.13; H: 5.25; N: 11.41; found: C: 39.05; H: 5.33; N: 11.37.

$[\mathrm{Co^{III}(prdioxH)(^{4Pyr}py)(Cl)}]\mathrm{PF_6}$ (2). $[\mathrm{Co^{III}(prdioxH)(Cl)_2}]$ (1 mmol, 0.369 g) was dissolved in 20 mL methanol. A solution of $\mathrm{KPF_6}$ (1.7 mmol, 0.3128 g) in 5 mL water was added to the solution followed by ^{4Pyr}pyridine (1 mmol, 0.148 g) in 5 mL of methanol. The reaction mixture was stirred for 2 h and then rotary-evaporated to 10 mL. This complex was extracted into dichloromethane ($\mathrm{CH_2Cl_2}$, the process was repeated 4 times). Petroleum ether was added to the $\mathrm{CH_2Cl_2}$ layer until the solution became turbid. After a few days, a reddish-brown precipitate was obtained. Yield: 60%. IR (KBr, $\mathrm{cm^{-1}}$) 3666 (w) (OH); 3115 (w) (aromatic-CH); 2958 (w), 2872 (w) (aliphatic CH); 1623 (s) (C=N); 1461 (m) (C=C); 835 (s) ($\mathrm{PF_6^-}$). ESI pos. in MeOH: m/z = 481.1563 for $[\mathrm{Co^{III}(prdioxH)(^{4Pyr}py)(Cl)}]^+$. Anal. calcd for $\mathrm{C_{20}H_{31}ClCoF_6N_6O_2P}$: C: 38.32; H: 4.98; N: 13.41; found: C: 38.25; H: 4.91; N: 13.36.

$[\mathrm{Co^{III}(prdioxH)(^{4Bz}py)(Cl)}]\mathrm{PF_6}$ (3). $[\mathrm{Co^{III}(prdioxH)(Cl)_2}]$ (1 mmol, 0.369 g) was dissolved in 20 mL methanol. A solution of $\mathrm{KPF_6}$ (1.7 mmol, 0.3128 g) in 5 mL water was added to the solution followed by ^{4Bz}pyridine (1 mmol, 0.183 g) in 5 mL of methanol. The reaction mixture was stirred for 2 hours and then, rotary-evaporated to 10 mL. This solution was kept for 4 days and brownish-yellow precipitate was recovered. X-ray quality crystals were obtained after recrystallization from ethanol/acetone (1 : 1) mixture. Yield: 80%. IR (KBr, $\mathrm{cm^{-1}}$) 3509 (w) (OH); 3141 (w), 3090 (w) (aromatic-CH); 2934 (w), 2850 (w) (aliphatic CH); 1674 (m) (C=O); 1613 (m), 1598 (m) (C=N); 1448 (m) (C=C); 840 (s) ($\mathrm{PF_6^-}$). ESI pos. in MeOH: m/z = 516.1207 for $[\mathrm{Co^{III}(prdioxH)(^{4Bz}py)(Cl)}]^+$. Anal. calcd for $\mathrm{C_{23}H_{28}ClCoF_6N_5O_3P}$: C: 41.74; H: 4.26; N: 10.58; found: C: 41.60; H: 4.30; N: 10.16.

Reduction of $[\mathrm{Co^{III}(prdioxH)(^{4tBu}py)(Cl)}]\mathrm{PF_6}$ (1) to $[\mathrm{Co^{I}(prdioxH)(^{4tBu}py)}]$ (4). This complex was synthesized by chemical reduction using standard glovebox techniques and decamethylcobaltocene as a reducing agent. The parent complex **1** was dissolved in dry THF and treated with two equivalents of decamethylcobaltocene. The resulting dark-blue solution was stirred for two hours and then dried under vacuum. The crude product was then washed with diethyl ether and further dried.

Acknowledgements

This research was made possible by the Division of Chemical Sciences, Geosciences, and Biosciences, Office of Basic Energy Sciences of the U.S. Department of Energy through the Single-Investigator and Small-Group Research (SISGR) – Solar Energy program grants DE-SC0001907 and DE-FG02-09ER16120 to C. N. V. and H. B. S., including financial support to D. B., S. M., H. B., D. W., and X. S. Work at the Argonne National Laboratory (J. N. and O. G. P.) was supported by the U.S. Department of Energy, Office of Science, Office of Basic Energy Sciences, Division of Chemical Sciences, Geosciences, and Biosciences, under contract number DE-AC02-06CH11357. D. B. and S. M. contributed equally to this work. We thank Prof. J. Endicott, WSU, for insightful discussions and suggestions. We also acknowledge the WSU-Computing Grid for high-level DFT calculations.

References

1 (*a*) J. A. Turner, *Science*, 2004, **305**, 972; (*b*) N. S. Lewis and D. G. Nocera, *Proc. Natl. Acad. Sci. U. S. A.*, 2006, **103**, 15729; (*c*) A. J. Esswein and D. G. Nocera, *Chem. Rev.*, 2007, **107**, 4022; (*d*) T. R. Cook, D. K. Dogutan, S. Y. Reece, Y. Surendranath, T. S. Teets and D. G. Nocera, *Chem. Rev.*, 2010, **110**, 6474; (*e*) M. G. Walter, E. L. Warren, J. R. McKone, S. W. Boettcher, Q. Mi, E. A. Santori and N. S. Lewis, *Chem. Rev.*, 2010, **110**, 6446; (*f*) P. D. Tran, V. Artero and M. Fontecave, *Energy Environ. Sci.*, 2010, **3**, 727; (*g*) J. R. McKone, S. C. Marinescu, B. S. Brunschwig, J. R. Winkler and H. B. Gray, *Chem. Sci.*, 2014, **5**, 865.

2 (*a*) Y. Sun, J. P. Bigi, N. A. Piro, M. L. Tang, J. R. Long and C. J. Chang, *J. Am. Chem. Soc.*, 2011, **133**, 9212; (*b*) J. P. Bigi, T. E. Hanna, W. H. Harman, A. Chang and C. J. Chang, *Chem. Commun.*, 2010, **46**, 958; (*c*) M. J. Rose, H. B. Gray and J. R. Winkler, *J. Am. Chem. Soc.*, 2012, **134**, 8310; (*d*) E. Deponti, A. Luisa, M. Natali, E. Iengo and F. Scandola, *Dalton Trans.*, 2014, **43**, 16345; (*e*) P. Zhang, M. Wang, F. Gloaguen, L. Chen, F. Quentelb and L. Sun, *Chem. Commun.*, 2013, **49**, 9455; (*f*) M. Natali, A. Luisa, E. Iengo and F. Scandola, *Chem. Commun.*, 2014, **50**, 1842; (*g*) C. Bachmann, B. Probst, M. Guttentag and R. Alberto, *Chem. Commun.*, 2014, **50**, 6737; (*h*) K. Kawano, K. Yamauchi and K. Sakai, *Chem. Commun.*, 2014, **50**, 9872; (*i*) W. M. Singh, M. Mirmohades, R. T. Jane, T. A. White, L. Hammarström, A. Thapper, R. Lomoth and S. Ott, *Chem. Commun.*, 2013, **49**, 8638; (*j*) J. Xie, Q. Zhou, C. Li, W. Wang, Y. Hou, B. Zhanga and X. Wang, *Chem. Commun.*, 2014, **50**, 6520; (*k*) Y. Sun, J. Sun, J. R. Long, P. Yang and C. J. Chang, *Chem. Sci.*, 2013, **4**, 118.

3 (*a*) L. A. Berben and J. C. Peters, *Chem. Commun.*, 2010, 398; (*b*) C. C. McCrory, L. C. Uyeda and J. C. Peters, *J. Am. Chem. Soc.*, 2012, **134**, 3164; (*c*) P. A. Jacques, V. Artero, J. Pecaut and M. Fontecave, *Proc. Natl. Acad. Sci. U. S. A.*, 2009, **106**, 20627; (*d*) M. Razavet, V. Artero and M. Fontecave, *Inorg. Chem.*, 2005, **44**, 4786; (*e*) C. Baffert, V. Artero and M. Fontecave, *Inorg. Chem.*, 2007, **46**, 1817; (*f*) A. Fihri,

V. Artero, M. Razavet, C. Baffert, W. Leibl and M. Fontecave, *Angew. Chem., Int. Ed.*, 2008, **47**, 564; (*g*) A. Fihri, V. Artero, A. Pereira and M. Fontecave, *Dalton Trans.*, 2008, 5567; (*h*) P. Du, J. Schneider, G. Luo, W. W. Brennessel and R. Eisenberg, *Inorg. Chem.*, 2009, **48**, 4952; (*i*) T. Lazarides, T. McCormick, P. Du, G. Luo, B. Lindley and R. Eisenberg, *J. Am. Chem. Soc.*, 2009, **131**, 9192; (*j*) T. M. McCormick, B. D. Calitree, A. Orchad, N. D. Kraut, F. V. Bright, M. R. Detty and R. Eisenberg, *J. Am. Chem. Soc.*, 2010, **132**, 15480; (*k*) T. M. McCormick, Z. Han, D. J. Weinberg, W. W. Brennessel, P. L. Holland and R. Eisenberg, *Inorg. Chem.*, 2011, **50**, 10660; (*l*) B. Probost, A. Rodenberg, M. Guttentag, P. Hamm and R. Alberto, *Inorg. Chem.*, 2010, **49**, 6453; (*m*) L. M. Utschig, S. C. Silver, K. L. Mulfort and D. M. Tiede, *J. Am. Chem. Soc.*, 2011, **133**, 16334; (*n*) K. L. Mulfort and D. M. Tiede, *J. Phys. Chem. B*, 2010, **114**, 14572; (*o*) C. Li, M. Wang, J. Pan, P. Zhang, R. Zhang and L. Sun, *J. Organomet. Chem.*, 2009, **694**, 2814; (*p*) F. Lakadamyali, M. Kato, N. M. Muresan and E. Reisner, *Angew. Chem., Int. Ed.*, 2012, **51**, 9381; (*q*) F. Lakadamyali and E. Reisner, *Chem. Commun.*, 2011, **47**, 1695; (*r*) J. Willkomm, N. M. Muresan and E. Reisner, *Chem. Sci.*, 2015, **6**, 2727.

4 (*a*) C. N. Valdez, J. L. Dempsey, B. S. Brunschwig, J. R. Winkler and H. B. Gray, *Proc. Natl. Acad. Sci. U. S. A.*, 2012, **109**, 15589; (*b*) S. C. Marinescu, J. R. Winkler and H. B. Gray, *Proc. Natl. Acad. Sci. U. S. A.*, 2012, **109**, 15127; (*c*) E. A. Mallart, C. Costentin, M. Fournier, S. Nowak, M. Robert and J. M. Saveant, *J. Am. Chem. Soc.*, 2012, **134**, 6104; (*d*) W. M. Singh, T. Baine, S. Kudo, S. Tian, X. A. N. Ma, H. Zhou, N. J. DeYonker, T. C. Pham, J. C. Bollinger, D. L. Baker, B. Yan, C. E. Webster and X. Zhao, *Angew. Chem., Int. Ed.*, 2012, **51**, 5941.

5 P. Connolly and J. H. Espenson, *Inorg. Chem.*, 1986, **25**, 2684.

6 (*a*) V. Artero, M. Chavarot-Kerlidou and M. Fontecave, *Angew. Chem., Int. Ed.*, 2011, **50**, 7238; (*b*) P. Du and R. Eisenberg, *Energy Environ. Sci.*, 2012, **5**, 6012; (*c*) M. Wang, L. Chen and L. Sun, *Energy Environ. Sci.*, 2012, **5**, 6763; (*d*) B. H. Solis and S. Hammes-Schiffer, *J. Am. Chem. Soc.*, 2011, **133**, 19036; (*e*) C. F. Leung, Y. Z. Chen, H. Q. Yu, S. M. Yiu, C. C. Ko and T. C. Lau, *Int. J. Hydrogen Energy*, 2011, **36**, 11640; (*f*) B. Solis, Y. Yu and S. Hammes-Schiffer, *Inorg. Chem.*, 2013, **52**, 6994; (*g*) J. T. Muckermann and E. Fujita, *Chem. Commun.*, 2011, **47**, 12456; (*h*) M. T. D. Nguyen, M. F. Charlot and A. Aukauloo, *J. Phys. Chem. A*, 2011, **115**, 911; (*i*) B. H. Solis and S. Hammes-Schiffer, *Inorg. Chem.*, 2011, **50**, 11252; (*j*) J. L. Dempsey, B. S. Brunschwig, J. R. Winkler and H. B. Gray, *Acc. Chem. Res.*, 2009, **42**, 1995; (*k*) J. L. Dempsey, J. R. Winkler and H. B. Gray, *J. Am. Chem. Soc.*, 2010, **132**, 16774; (*l*) A. E. King, Y. Surendranath, N. A. Piro, J. P. Bigi, J. R. Long and C. J. Chang, *Chem. Sci.*, 2013, **4**, 1578; (*m*) A. Bhattacharjee, E. S. Andreiadis, M. C. Kerlidou, M. Fontecave, M. J. Field and V. Artero, *Chem.–Eur. J.*, 2013, **19**, 15166; (*n*) M. Nippe, R. S. Khnayzer, J. A. Panetier, D. Z. Zee, B. S. Olaiya, M. Head-Gordon, C. J. Chang, F. N. Castellano and J. R. Long, *Chem. Sci.*, 2013, **4**, 3934.

7 A. Gerli and L. G. Marzilli, *Inorg. Chem.*, 1992, **31**, 1152.

8 S. Shi, L. M. Daniels and J. H. Espenson, *Inorg. Chem.*, 1991, **30**, 3407.

9 X. Hu, B. S. Brunschwig and J. C. Peters, *J. Am. Chem. Soc.*, 2007, **129**, 8988.

10 (*a*) R. Shakya, C. Imbert, H. P. Hratchian, M. Lanzaster, M. J. Heeg, B. R. McGarvey, M. Allard, H. B. Schlegel and C. N. Verani, *Dalton Trans.*, 2006, **21**, 2517; (*b*) R. Shakya, S. S. Hindo, L. Wu, M. Allard, M. J. Heeg, H. P. Hratchian, B. R. McGarvey, S. R. P. Da Rocha and C. N. Verani, *Inorg. Chem.*, 2007, **46**, 9808; (*c*) F. D. Lesh, R. L. Lord, M. J. Heeg, H. B. Schlegel and C. N. Verani, *Eur. J. Inorg. Chem.*, 2012, **03**, 463; (*d*) M. M. Allard, F. R. Xavier, M. J. Heeg, H. B. Schlegel and C. N. Verani, *Eur. J. Inorg. Chem.*, 2012, 4622; (*e*) D. Basu, M. M. Allard, F. R. Xavier, M. J. Heeg, H. B. Schlegel and C. N. Verani, *Dalton Trans.*, 2015, **44**, 3454; (*f*) D. Basu, S. Mazumder, X. Shi, H. Baydoun, J. Niklas, O. Poluektov, H. B. Schlegel and C. N. Verani, *Angew. Chem., Int. Ed.*, 2015, **54**, 2105; (*g*) D. Basu, S. Mazumder, X. Shi, R. Staples, H. B. Schlegel and C. N. Verani, *Angew. Chem., Int. Ed.*, 2015, **54**, 7139.

11 E. Uhlig and M. Friedrich, *Z. Anorg. Allg. Chem.*, 1966, **343**, 299.

12 G. Costa, G. Mestroni and E. D. Savorgnani, *Inorg. Chim. Acta*, 1969, 323.

13 A. Bhattacharjee, M. Chavarot-Kerlidou, E. S. Andreiadis, M. Fontecave, M. J. Field and V. Artero, *Inorg. Chem.*, 2012, **51**, 7087.

14 (*a*) M. Rangel, A. Leite, J. Gomes and B. Castro, *Organometallics*, 2005, **24**, 3500; (*b*) J. Niklas, K. L. Mardis, R. R. Rakhimov, K. L. Mulfort, D. M. Tiede and O. G. Poluektov, *J. Phys. Chem. B*, 2012, **116**, 2943.

15 (*a*) M. D. Wirt, C. J. Bender and J. Peisach, *Inorg. Chem.*, 1995, **34**, 1663; (*b*) J. Hermer, S. V. Doorslaer, I. Gromov and A. Schweiger, *Chem. Phys. Lett.*, 2002, **358**, 8.

16 T. J. R. Weakley, J. Marks and R. G. Finke, *Acta Crystallogr., Sect. C: Cryst. Struct. Commun.*, 1994, **50**, 1690.

17 D. C. Lacy, G. M. Roberts and J. C. Peters, *J. Am. Chem. Soc.*, 2015, **137**, 4860.

18 V. Fourmond, P. A. Jacques, M. Fontecave and V. Artero, *Inorg. Chem.*, 2010, **49**, 10338.

19 D. P. Estes, D. C. Grills and J. R. Norton, *J. Am. Chem. Soc.*, 2014, **136**, 17362.

20 R. Gagne, C. Koval and G. Licenski, *Inorg. Chem.*, 1980, **19**, 2854.

21 (*a*) *COSMO V1.58, Software for the CCD Detector Systems for Determining Data Collection Parameters. Bruker Analytical X-ray Systems*, Madison, WI, 2008; (*b*) *APEX2 V2008.5-0 Software for the CCD Detector System; Bruker Analytical X-ray Systems*, Madison, WI, 2008; (*c*) *SAINT V 7.34 Software for the Integration of CCD Detector System Bruker Analytical X-ray Systems*, Madison, WI, 2008; (*d*) SADABS V2.008/2 Program for absorption corrections using Bruker-AXS CCD based on the method of Robert Blessing; R. H. Blessing, *Acta Crystallogr., Sect. A: Found. Crystallogr.*, 1995, **A51**, 33;

(*e*) G. M. Sheldrick, A short history of SHELX, *Acta Crystallogr., Sect. A: Found. Crystallogr.*, 2008, **64**, 112; (*f*) P. V. D. Sluis and A. L. Spek, *Acta Crystallogr., Sect. A: Found. Crystallogr.*, 1990, **46**, 194; (*g*) A. L. Spek, *J. Appl. Crystallogr.*, 2003, **36**, 7, [a]Obtained with graphite monochromated Mo Kα ($l = 0.71073$ Å) radiation. [b]$R_1 = \sum||F_o|-|F_c||/\sum|F_o|$. [c]$wR_2 = \{\sum[w(F_o^2 - F_c^2)^2/\{\sum[w(F_o^2)^2]\}^{1/2}$; (*h*) *COSMO V1.61, Software for the CCD Detector Systems for Determining Data Collection Parameters. Bruker Analytical X-ray Systems*, Madison, WI, 2009; (*i*) *APEX2 V2010.11-3. Software for the CCD Detector System; Bruker Analytical X-ray Systems*, Madison, WI, 2010; (*j*) *SAINT V 7.68A Software for the Integration of CCD Detector System Bruker Analytical X-ray Systems*, Madison, WI, 2010; (*k*) O. V. Dolomanov, L. J. Bourhis, R. J. Gildea, J. A. K. Howard and H. Puschmann, OLEX2: a complete structure solution, refinement and analysis program, *J. Appl. Crystallogr.*, 2009, **42**, 339.

22 (*a*) M. J. Frisch, G. W. Trucks and H. B. Schlegel, *et al.*, *Gaussian Development Version; Revision H.35 ed.*, Gaussian, Inc., Wallingford, CT2010; (*b*) A. D. Becke, *J. Chem. Phys.*, 1993, **98**, 5648; (*c*) J. P. Perdew, *Phys. Rev. B: Condens. Matter Mater. Phys.*, 1986, **33**, 8822; (*d*) J. P. Perdew, K. Burke and Y. Wang, *Phys. Rev.*, 1996, **54**, 16533; (*e*) T. H. Dunning Jr and P. J. Hay, in *Modern Theoretical Chemistry*, ed. H. F. Schaefer III, Plenum, New York, 1977, vol. 3, pp. 1–28; (*f*) M. Dolg, H. Wedig and H. Preuss, *J. Chem. Phys.*, 1987, **86**, 866; (*g*) S. Miertus, E. Scrocco and J. Tomasi, *J. Chem. Phys.*, 1981, **55**, 117; (*h*) G. Scalmani and M. J. Frisch, *J. Chem. Phys.*, 2010, **132**, 114110; (*i*) G. Scalmani, M. J. Frisch, B. Mennucci, J. Tomasi, R. Cammi and V. Barone, *J. Chem. Phys.*, 2006, **124**, 9410; (*j*) J. Tomasi, B. Mennucci and R. Cammi, *Chem. Rev.*, 2005, **105**, 2999; (*k*) A. Schaefer, C. Huber and R. Ahlrichs, *J. Chem. Phys.*, 1994, **100**, 5829; (*l*) R. Krishnan, J. S. Binkley, R. Seeger and J. A. Pople, *J. Chem. Phys.*, 1980, **72**, 650; (*m*) R. Seeger and J. A. Pople, *J. Chem. Phys.*, 1977, **66**, 3045; (*n*) H. B. Schlegel and J. J. McDouall, *Computational Advances in Organic Chemistry*, ed. C. Ögretir and I. G. Csizmadia, Kluwer Academic, Amsterdam, The Netherlands, 1991; (*o*) R. Bauernschmitt and R. Ahlrichs, *J. Chem. Phys.*, 1996, **104**, 9047; (*p*) R. Pennington, T. Keith and J. M. Millam, *GaussView V. 5.0*, Semichem, Inc., Shawnee Mission, KS, 2009.